Electronic Structure and Charge Transport Properties of a Series of 3,6-(Diphenyl)-*s*-tetrazine Derivatives; Are They Suitable Candidates for Molecular Electronics?

Mónica Moral,[1] Gregorio García,[2] Andrés Garzón,[3] José M. Granadino-Roldán,[1] Mark A. Fox,[4] Dmitry S. Yufit,[4] Antonio Peñas,[5] Manuel Melguizo[5] and Manuel Fernández-Gómez[1,]*

[1] Department of Physical and Analytical Chemistry, Faculty of Experimental Sciences, University of Jaén. Campus Las Lagunillas, E23071, Jaén, Spain

[2] Department of Chemistry, University of Burgos. Plaza Misa el Bañuelos s/n 09001 Burgos, Spain

[3] Department of Physical Chemistry, Faculty of Pharmacy, University of Castilla-La Mancha. Paseo de Los Estudiantes, E02071, Albacete, Spain

[4] Department of Chemistry. University of Durham, South Road, Durham, DH1 3LE, U.K.

[5] Department of Inorganic and Organic Chemistry, Faculty of Experimental Sciences, University of Jaén. Campus las Lagunillas, E23071, Jaén, Spain

KEYWORDS: Halo and cyano 3,6-diphenyl-*s*-tetrazines – Opto-electronic properties – Organic Semiconductor – Electron Transfer – Marcus-Levich-Jortner Model.

ABSTRACT

Opto-electronic and charge-transport related properties of a series of 3,6-diphenyl-*s*-tetrazine derivatives, including F, Cl, Br and CN substituents, have been analyzed. The molecular structure and electronic properties of the new fluorine-containing derivative, bis(3,6-difluorophenyl)-*s*-tetrazine, were explored by spectroscopic, electrochemical and theoretical methods. The effect of the substituent on the pristine compound have been assessed from a theoretical perspective, showing that the fluorinated and brominated derivatives have the highest predicted electron mobilities, while the cyano derivative is foreseen to undergo the most efficient electron injection process.

INTRODUCTION

Tetrazine derivatives constitute the most electron-deficient aromatic family[1-3] and display interesting properties as concern semiconducting and opto-electronic applications, *e.g.* redox reversibility on reduction and exhibit low potentials[2,4,5] and also they are coloured due to a n $\rightarrow \pi^*$ low energy transition.[5-8] In addition, several tetrazine derivatives are fluorescent in the visible wavelength region, λ_{max} ~ 550-570 nm).[9-11] Desirable electronic properties have been described for 3,6-diphenyl-*s*-tetrazine (Ph_2Tz, Chart 1) and some other diaryl derivatives[3,4,7,8,12,13] which leads us to consider this family of compounds as suitable candidates for *n*-type semiconducting materials. A proven strategy to improve the *n*-type semiconductor properties is by functionalizing with electron-withdrawing substituents, such as F, Cl, Br and CN, since they increase the electron affinity and lower the electron injection barrier.[14-19] These factors allow the use of more stable cathodes such as aluminum instead of the more reactive calcium (more prone to atmospheric degradation).[14-21]

The effect of attaching such electron-withdrawing substituents on charge-transport properties has been analyzed elsewhere (see, *e.g.* 14, 21-26). Perfluoro-pentacene constitutes a nice example as it exhibits electron mobility (μ) values as high as 0.22 $cm^2\ V^{-1}\ s^1$ and the combination of perfluoropentacene (*n*-channel) and pentacene (*p*-channel) yields high-performance *p-n* junctions and offers the possibility to fabricate bipolar transistors.[23]

In the present work we first analyze from a theoretical point of view, the effect caused by F, Cl, Br and CN substitution (Chart 1) on the opto-electronic properties and *n*-type semiconductor character of the parent molecule, Ph_2Tz.[8] Besides, the molecular structure and electronic properties of bis(3,5-difluorophenyl)-*s*-tetrazine, $(F_2Ph)_2Tz$ (see Chart 1), were analyzed by spectroscopic, structural, electrochemical and theoretical

methods. The electron transport properties were evaluated on molecular crystals modeled from the X-ray crystal structure of $(F_2Ph)_2Tz$.

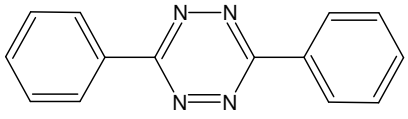

Ph_2Tz

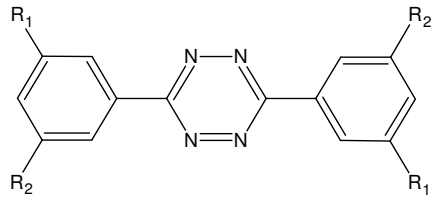

$R_1 = F$	$R_2 = F$	$(F_2Ph)_2Tz$
$R_1 = F$	$R_2 = H$	$(FPh)_2Tz$
$R_1 = Cl$	$R_2 = Cl$	$(Cl_2Ph)_2Tz$
$R_1 = Cl$	$R_2 = H$	$(ClPh)_2Tz$
$R_1 = Br$	$R_2 = Br$	$(Br_2Ph)_2Tz$
$R_1 = CN$	$R_2 = CN$	$((NC)_2Ph)_2Tz$

Chart 1. Chemical formulae of 3,6-diphenyl-*s*-tetrazine and some derivatives.

EXPERIMENTAL SECTION

General. All reagents were of commercial quality and solvents were dried using standard procedures. ^1H and ^{13}C-NMR spectra were recorded in a Bruker Avance 400 and a Bruker Avance 500 spectrophotometers. The mass spectra were recorded with a high resolution mass spectrometer Waters Micromass AutoSpec NT.

Synthesis. The synthesis of bis(3,5-difluorophenyl)-*s*-tetrazine, $(F_2Ph)_2Tz$, was performed via a Pinner-type reaction between 3,5-difluorobenzonitrile and hydrazine,[8,27] with N-acetylcysteine as catalyst (Scheme S1). Hydrazine hydrate (2.9 mL, 58.46 mmol) was dropwise added to a solution of 3,5-difluorobenzonitrile (2 mL, 58.46 mmol) and N-acetylcysteine (3.3 g, 19.49 mmol) in MeOH (20 mL) at room temperature, and the resulting mixture was stirred for 24 h at reflux temperature under

Ar atmosphere. Then, the solvent was removed under reduced pressure and the solid residue was distributed between 15% NaOH aqueous solution and dichloromethane. The organic layer was dried over anhydrous Na_2SO_4 and evaporated under reduced pressure to give a reddish solid. This solid was dissolved in methanol and the resulting clear solution was stirred for 12 h in an open vessel at room temperature. Then, the red solid in suspension was collected by filtration, washed with methanol and dried under vacuum to afford 2 (see Scheme S1) with a 79 % yield (referred to 3,5-difluorobenzonitrile) as a spectroscopically pure red crystalline solid. ^{1}H NMR (400 MHz, $CDCl_3$) δ ppm 7.12 (tt, *J* = 8.48, 2.38 Hz, 2 H), 8.21 (m, 4 H). $^{13}C\{^{1}H\}$ NMR (101 MHz, $CDCl_3$) δ ppm 108.44 (t, *J* = 25.7 Hz), 111.19 (m), 134.60 (t, *J* = 10.2 Hz), 162.98 (t, *J* = 3.6 Hz), 163.67 (dd, *J* = 249.4, 13.2 Hz). $^{13}C\{^{19}F\}$ NMR (126 MHz, $CDCl_3$) δ ppm 108.44 (d, *J* = 167.5 Hz), 111.18 (d, *J* = 168.5 Hz), 134.58 (s), 162.88 (s), 163.66 (s). HRMS (DIP/EI): Exact mass calcd. for $C_{14}N_4H_6F_4$: 306.0529; found: 306.0531.

Spectroscopy. FTIR spectra were recorded both in solid phase (in KBr discs) and in CCl_4 solution at a resolution of 1 cm^{-1} and 200 scans with a Bruker Vector 22 spectrophotometer. ATR-FTIR spectrum was recorded at the same resolution in a Jasco 4100 spectrophotometer. Raman spectra in solid phase and in CCl_4 solution were recorded with a Bruker RFS 100/S FT-Raman spectrophotometer at a resolution of 1 cm^{-1}, 150 scans and laser power between 250 mW (for liquid phase) and 500 mW (for the solid phase). The liquid-phase Raman spectra were also recorded with polarized light at 0º and 90º. UV–Vis absorption spectra were recorded in chloroform, carbon tetrachloride, methanol and *n*-hexane as solvents with a Varian Cary 4000 spectrophotometer with a resolution of 1 nm.

Single crystal X-Ray crystallography. The single crystal X-ray data for compounds Ph_2Tz and $(F_2Ph)_2Tz$ have been collected on a Bruker SMART CCD 6000 diffractometer (graphite monochromator, λMoKα, λ = 0.71073Å) equipped with a Cryostream (Oxford Cryosystems) open-flow nitrogen cryostats at the temperature 120.0(2) K. All structures were solved by direct method and refined by full-matrix least squares on F^2 for all data using Olex2[28] and SHELXTL[29] software. All non-hydrogen atoms were refined anisotropically, hydrogen atoms were refined isotropically. Crystal data and parameters of refinement are listed in Table S1. Crystallographic data for the structure have been deposited with the Cambridge Crystallographic Data Centre as supplementary publication CCDC-992614-992615.

Electrochemical methods. Cyclic voltammetry measurements (Autolab PG-STAT 30) were carried out using dry dichloromethane or acetonitrile solutions containing 0.1 M NBu_4PF_6 electrolyte in a standard three-electrode cell using a glassy carbon (2 mm diameter disc) working electrode with platinum wires as counter and reference electrodes. Potentials are reported using an internal ferrocenium/ferrocene couple (FcH^+/FcH = 0.0 V) as reference. All electrochemical experiments were carried out in a nitrogen atmosphere at ambient temperatures.

Spectroelectrochemical experiments were performed at room temperature in an airtight optically transparent thin-layer electrochemical (OTTLE) cell equipped with Pt minigrid working and counter electrodes (32 wires cm^{-1}), Ag wire pseudo-reference electrode and CaF_2 windows for a 200 μm path-length solvent compartment.[30] The cell was positioned in the sample compartment of a Perkin-Elmer Lambda-900 spectrophotometer. An initial potential was applied such that no electrochemical work was done. The applied potential was then increased in a small (50 - 100 mV) step and the system allowed to reach equilibrium, as determined by both the decrease in current

flowing through the cell and the reproducibility of spectra *vs.* time, before further increase in applied potential. When complete electrolysis had been achieved (as determined by the relative changes in the spectroscopic profile), the chemical reversibility was determined by back oxidation using a similar sequence of controlled potential steps. The controlled-potential electrolyses were carried out using an Autolab PG-STAT 30 potentiostat.

THEORETICAL AND COMPUTATIONAL METHODOLOGY

Electron injection and transport: theoretical considerations. High performances in *n*-type organic semiconductors are related to electron injection easiness as well as high charge carrier mobilities.[31-33] Low-energy LUMO levels and sufficiently high electron affinities are needed for efficient charge injections.[20,31] The height of the potential barrier, i.e. the energy difference between the LUMO level and the work function (Φ_i) of the metal electrode is an essential factor which controls the efficiency of the process.[34-37] This energy difference of less than 0.2-0.3 eV is generally accepted for an ohmic contact between semiconductor material and electrode to take place[36,37] neglecting effects involving metal reactivity, interdiffusion within the metal-organic interface and temperature.[31] Electron affinity (EA), defined as the energy released when one electron is added to the system in the gaseous state, is also of great importance for a material to be considered as *n*-type semiconductor. It should be high enough to allow efficient injection of electrons into the empty LUMO although if the molecule is too electrophilic its ambient stability could be compromised.[31]

In typical π-conjugated organic crystal materials with small bandwidths (< 1 eV) at room temperature, charge motion is generally produced by a hopping mechanism. This mechanism can be described as a self-exchange electron-transfer (ET) reaction

between neighboring molecules within the framework of the Marcus-Levich-Jortner (MLJ) model.[38,39] Accordingly, the rate constant for electron transfer (k_{ET}) can be expressed as:

$$k_{ET} = \frac{2\pi}{\hbar} t_{12}^2 \sqrt{\frac{1}{4\pi\lambda_0 k_B T}} \sum_{n=0}^{\infty} \left[exp\left(-S_{eff}^n\right) \times \frac{S_{eff}^n}{n!} \times exp\left(\frac{-\left(\lambda_0 + n\hbar\omega_{eff} + \Delta G^0\right)^2}{4\lambda_0 k_B T} \right) \right]$$

(1)

where k_B is Bolztmann's constant and T is the temperature, fixed at 300 K, t_{12} and λ_0 stand for charge transfer integral and the classical contribution (mostly the external) to the reorganization energy fixed at 0.1 eV, respectively. Generally, in organic crystals the outer contribution is in the order of a tenth of an electronvolt as opposite to charge transfer in solution wherein the external part dominates.[18,31,40-42] ΔG^0 is the energy difference between the electronic states involved in the charge transfer process (equal to zero in the self-exchange process), $S_{eff} = \lambda_i/\hbar\omega_{eff}$ is the effective Huang-Rhys factor, λ_i, the inner reorganization energy, and ω_{eff}, the frequency of the effective vibrational mode assisting the process, fixed at $\hbar_{eff} \sim 0.2$ eV. The inner reorganization energy, λ_i, for self-exchange consists of two terms corresponding to the geometry relaxation energies upon going from the neutral-state geometry to the charged-state one and *vice versa*

$$\lambda_i = \lambda_1 + \lambda_2 \quad (2)$$

$$\lambda_1 = E^0(G^*) - E^0(G^0) \quad (3)$$

$$\lambda_2 = E^*(G^0) - E^*(G^*) \quad (4)$$

where $E^0(G^0)$ and $E^*(G^*)$ are the ground-state energies of the neutral and ionic states, respectively. $E^0(G^*)$ is the energy of the neutral molecule at the optimal ionic geometry; $E^*(G^0)$ is the energy of the charged state at the optimal geometry of the neutral molecule.[18,40-42]

The charge transfer integral, t_{12}, reflects the strength of the electronic interactions between neighboring molecules, so it critically depends on their relative spatial arrangement. The electronic coupling is defined by the matrix element

$$t_{12} = \langle \psi_1 | H | \psi_2 \rangle \quad (5)$$

where H is the electronic Hamiltonian of the whole system and ψ_1 and ψ_2 are the wavefunctions of two initial and final charge-localized states.[32,42,43]

For an n-dimensional and spatially isotropic system, in which homogeneous charge diffusion can be assumed, D can be evaluated as:

$$D = \frac{1}{2n} \lim_{t \to \infty} \frac{\langle r^2 \rangle}{t} \approx \frac{1}{2n} \sum_i r_i^2 k_i p_i \quad (6)$$

where n = 3 and i runs over all nearest adjacent molecules while r_i, k_i are, respectively, the corresponding center-to-center hopping distance and the electron transfer rate constant (obtained from eqn. (1)), and p_i is the hopping probability calculated as by:[21,32,44]

$$p_i = \frac{k_i}{\sum_i k_i} \quad (7)$$

In the low field limit, the charge carrier mobility (μ_{hop}) can be described by the Einstein's relation

$$\mu_{hop} = \frac{eD}{k_B T} \quad (8)$$

where T is the temperature, k_B is the Boltzmann constant, e is the electron charge and D is the diffusion coefficient.[21,32,44]

Computational methods. DFT (B3LYP[45,46] and PBE0[47,48]) methods as implemented in Gaussian09 (revision **B.01**)[49] were used for the different calculations of molecular structures, vibrational frequencies and electronic properties described below. Concretely, infrared and Raman spectra were assigned using the harmonic vibrational frequency scale factors reported by Merrick et al.[50] on the basis of vibrational

frequencies calculated at the B3LYP/6-31+G* level on a structure optimized at the same level of theory within the isolated molecule approximation. Electronic transitions were analyzed at the time-dependent (TD)-PBE0/6-31+G* level for both the isolated and solvated molecule within the Polarizable Continuum Model (PCM) methodology.[51,52] TD-PBE0 has already been successfully employed to predict the electronic excitation spectrum of Ph_2Tz^8 and other conjugated organic compounds[53,54] as well as to calculate low-energy transitions for conjugated organic compounds when solvent effects are taken into account through the PCM approach.[55] PCM/TD-PBE0/6-31+G* calculations were carried out on molecular structures calculated at both the PCM/PBE0/6-31+G* level and the PCM/MP2/6-31+G* level (Møller-Plesset second order perturbation theory).[56-59] Both methods were employed in order to assess the over-planarity usually rendered by DFT methods for conjugated molecules and the effect on its electronic spectrum.[60,61]

Semiconducting related properties (E_{LUMO}, EA, λ_i and t_{12}) were calculated at the B3LYP/6-31+G* level of theory. Although Koopman's theorem is not rigorously applicable to Kohn-Sham orbital energies, Perdew proved a connection between ionization potentials/electron affinities and HOMO/LUMO energies through Janak's theorem (see, e.g. ref. 62-64 and references therein). In this sense, B3LYP has been proven to be accurate enough for predicting EAs[65,66] and provides theoretical λ_i values in good quantitative agreement with the experimental ones from gas-phase ultraviolet photoelectron spectroscopy.[67] Zhang and Musgrave have also reported B3LYP yields lower errors in the LUMO energy calculation of small organic molecules than other DFT methods with a higher percentage of HF Exchange.[68] The 6-31+G* basis set is recommended in calculations involving anionic species.[64]

Crystal structures were modeled with PBE[47] and a numerical double-ζ + polarization atomic orbital basis set, where the ions are described with norm-conserving Troullier-Martins pseudopotentials, as well as with PBE using a Grimme`s dipersion correction term[69] with a DZP basis set, PBE-D/DZP using the SIESTA code.[70] All the atomic positions and lattice parameters were relaxed using the conjugated gradient minimization method. The X-ray structures obtained in this study were used as starting points to model the Ph_2Tz and $(F_2Ph)_2Tz$ crystals. For the remaining compounds, i.e. $(Cl_2Ph)_2Tz$, $(Br_2Ph)_2Tz$ and $((NC)_2Ph)_2Tz$, crystal structures based on the modeled $(F_2Ph)_2Tz$ crystal were employed as the starting points. Afterwards, the electronic coupling parameter t_{12} was calculated for the different couples of molecules extracted from both the X-ray structures and the modeled crystals. Thus, the effect that deviations between experimental and theoretical structures lead on calculated charge-transport related properties was also evaluated. Charge transfer integrals were obtained following the so-called projective method,[71,72] according to which Fock's matrix is written in terms of localized orbitals by using the orbital projection, *i.e.* the molecular orbitals (MOs) of the selected dimer of stacked molecules are projected on a basis set defined by the MOs of the individual molecules. These calculations were carried out with the *J-from-g03* code.[71,72]

RESULTS AND DISCUSSION

Molecular structure. Both $(F_2Ph)_2Tz$ and Ph_2Tz yielded crystals suitable for X-ray diffraction analysis. Although the crystal structure of Ph_2Tz was first reported long ago by Ahmed and Kitaigorodsky,[73] it became necessary to update it in a more accurate fashion for comparison with the current data here computed. In Supplementary Material, Figures S1 and S2, Chart S1 and Tables S3-S9 summarize some of the most

relevant determined molecular parameters along with the calculated ones for the five molecular crystals. The calculated molecular structures are in agreement with the X-ray crystal structures. The substituents (halogen or CN) do not induce significant changes on the molecular parameters of the tetrazine ring and the inter-ring C-C lengths (1.48 – 1.49 Å). Nevertheless, the calculated dihedral angle between phenyl and tetrazine rings gradually increases from 13º for $(F_2Ph)_2Tz$ to 18º for $(CN_2Ph)_2Tz$, while the Ph_2Tz structure is nearly planar.

The calculated and experimental values for Ph_2Tz and $(F_2Ph)_2Tz$ of the lattice and π-stacking parameters in Table 1 are in agreement. The Ph_2Tz crystal shows a herringbone disposition while in the $(F_2Ph)_2Tz$ crystal, the stacks of molecules are T-shaped (see figure 1). These results parallel those reported for the crystals of pentacenes, where a change in the crystal configuration is observed on going from the parent pentacene to the perfluorinated pentacene.[14,23,74] As also reported for these pentacene crystals, a better cofacial stacking (see figure 1) is obtained with fluorine atoms which, in turn, improves the electronic couplings (see below). Some authors relate the higher planarity of Ph_2Tz in the crystal to weak C–H…N interactions ($d_{H...N}$ = 2.70 and 2.83 Å) between coplanar molecules.[75,76] In the $(F_2Ph)_2Tz$ crystal, weak C–F…H–C ($d_{F...H} \geq 2.65$ Å) intermolecular interactions between neighboring molecules may also play a role in the perpendicular dispositions found. The centroid-to-centroid (CCD) and plane-to-plane shift (PPS) distances increase as a function of the substituent size from F to CN. The plane-to-centroid (PCD) distances between two phenyl groups also increase from F to CN but the PCD values between the tetrazine rings keep constant.

It is well known that local, gradient corrected functionals, like PBE, show shortcomings at the adequate description of long-range (dispersion) interaction forces

that are commonly believed to be important in organic molecular crystals. However, the internal geometries of crystals are well reproduced here by PBE calculations (mean absolute error, MAE, for lattice parameters, 0.120 Å / 0.28(5)º as compared to 0.288 Å / 1.32(3)º obtained at PBE-D level, see Table S10 in Supplementary Information) which can be due either to van der Waals interactions may not be the most important driving forces for the bonding within these compounds,[77,78] or to a fortuitous cancellation of errors or a combination of both.

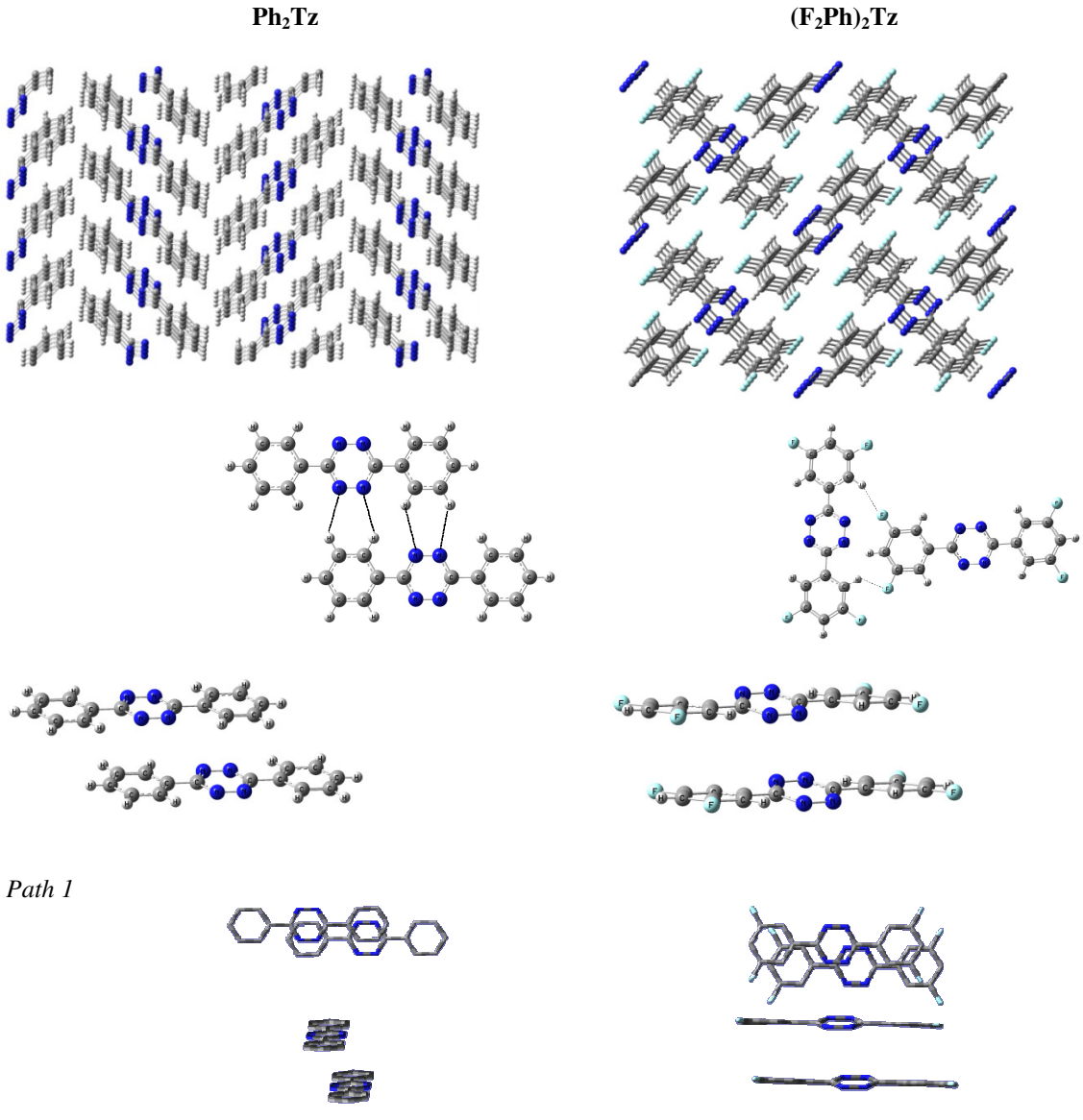

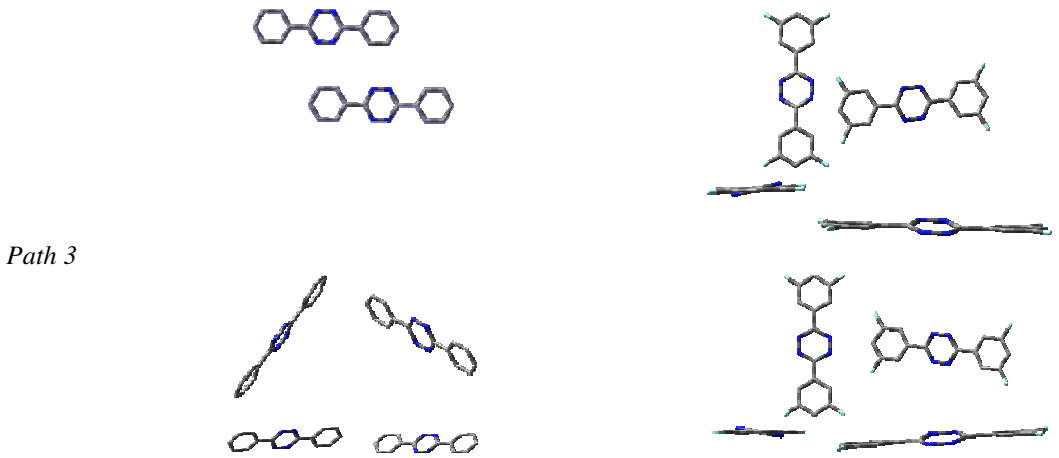

Figure 1. Molecular arrangements from the X-ray crystal structures (upper part) and different views for the most significant charge transport pathways in Ph_2Tz and $(F_2Ph)_2Tz$ (lower part). The remaining $(X_2Ph)_2Tz$ derivatives show similar pathways as $(F_2Ph)_2Tz$.

Table 1. Crystallographic and calculated lattice parameters (a, b, c, α, β and γ) for the unit cell along with the π stacking parameters between cofacial neighboring molecules.

	Compound						
	Ph_2Tz		**$(F_2Ph)_2Tz$**		**$(Cl_2Ph)_2Tz$**	**$(Br_2Ph)_2Tz$**	**$((CN)_2Ph)_2Tz$**
Lattice parameters	*Exp.*	*Theor.*	*Exp.*	*Theor.*	*Theor.*	*Theor.*	*Theor.*
a / Å	5.3913(5)	5.5447	3.7602(2)	3.7708	4.0504	4.1760	4.7335
b / Å	5.0992(5)	5.1918	14.1127(7)	14.1215	14.4802	14.8416	14.5545
c / Å	20.003(2)	20.331	11.8838(6)	12.0108	12.2341	12.4175	11.2946
α / degrees	90.0	90.0	90.0	90.24	90.30	90.02	90.27
β / degrees	92.67(2)	91.639	90.58(2)	90.41	92.40	91.50	86.29
γ / degrees	90.0	90.0	90.0	89.70	89.50	89.94	89.72
π stacking parameters							
PCD (Ph-Tz)	3.431(1) 3.072(2)	3.42 3.34					
PCD (Ph-Ph)			3.311(2)	3.45	3.73	3.73	3.80
PCD (Tz-Tz)			3.311(2)	3.14/3.16	3.21/3.28	3.17/3.20	3.13/3.19
CCD (Ph-Tz)	3.760(2) 3.760(2)	3.67 3.69					
CCD (Ph-Ph)			3.620(1)	3.77	4.05	4.18	4.73
CCD (Tz-Tz)			3.620(1)	3.77	4.05	4.18	4.73

PPS (Ph-Tz)	1.538(2) 2.169(2)	1.36 1.54					
PPS (Ph-Ph)			1.485(4)	1.52	1.57	1.87	2.83
PPS (Tz-Tz)			1.485(4)	2.05/2.08	2.38/2.47	2.68/2.72	3.50/3.55

PCD = plane-to-centroid distance, CCD = centroid-to-centroid distance, PPS = plane-to-plane shift.

Infrared and Raman spectroscopy. IR and Raman spectra recorded for $(F_2Ph)_2Tz$ in both solid (in KBr discs and by Attenuated Total Reflectance) and liquid (CCl_4 solvent) phases are collected in figures 2, S3 and S4. The assignment of the most characteristic bands and the depolarization ratios for the liquid-phase Raman spectrum of $(F_2Ph)_2Tz$ appear in Table S9. For brevity, only those vibrational assignments related to the most relevant aspects of the molecular structure and the effect of the halogen substituents are discussed here. In Table S9, a blue shift of the C-H stretching vibrations from (3074 – 3019) cm^{-1} to 3096 cm^{-1} (in CCl_4) can be seen with respect to the parent molecule Ph_2Tz. This shift can be linked to a shortening of the C-H distances due to the presence of the F atoms as predicted by B3LYP/6-31G* i.e. from (1.084 – 1.087) Å for Ph_2Tz to (1.082 – 1.083) Å for $(F_2Ph)_2Tz$. Inter-ring C-C stretching vibrations appear as a set of non-homogeneous intensity bands in the range (1476 – 1214) cm^1, in between that for a typical C-C (900 cm^{-1}) and a C=C (1650 cm^{-1}) stretching.[79] B3LYP predicts a D_{2h} planar structure for $(F_2Ph)_2Tz$, as for Ph_2Tz. Depolarization ratios measured for four bands assigned to mainly A_g stretching and bending motions lie in the range 0.34 – 0.55. They are somewhat higher than those for Ph_2Tz (0.17 – 0.41) which may suggest that $(F_2Ph)_2Tz$ departs from D_{2h} symmetry in liquid phase more than Ph_2Tz does.

(a)

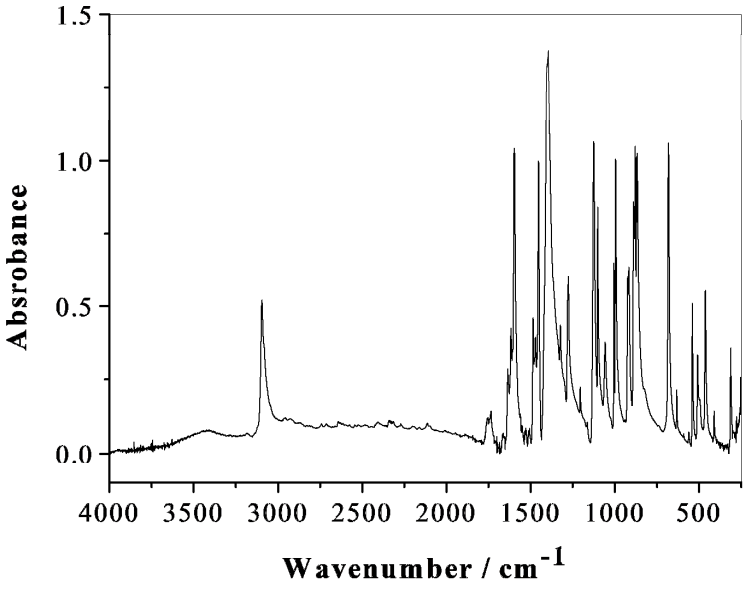

(b)

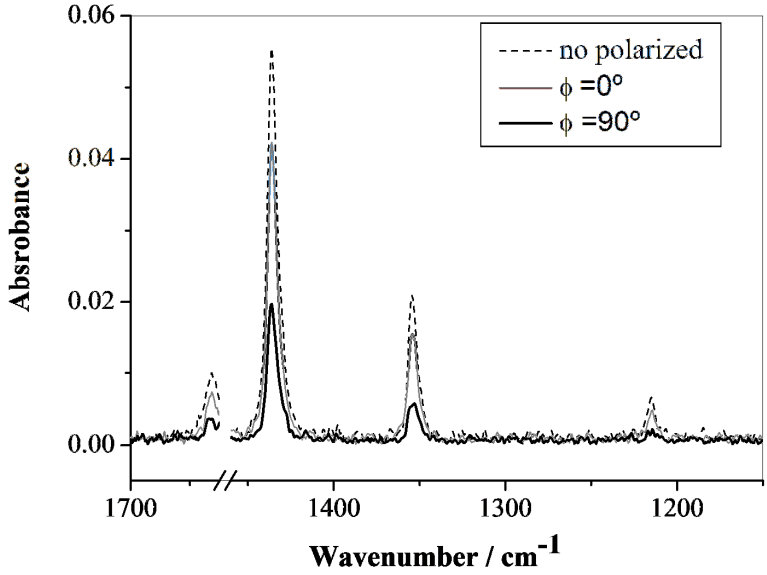

Figure 2. (a) IR spectrum of $(F_2Ph)_2Tz$ in KBr discs; (b) Raman spectra of $(F_2Ph)_2Tz$ in CCl_4 solution recorded with and without polarization at 0º and 90º.

Electrochemical response. As expected for tetrazine derivatives,[2,4,5] both Ph_2Tz and $(F_2Ph)_2Tz$ show reversible reduction waves at low potentials in CH_3CN solutions. (Figure S5 and Table 2). Reduction potentials for the difluorinated and dichlorinated derivatives of Ph_2Tz, i.e. $(FPh)_2Tz$ and $(ClPh)_2Tz$ (Chart 1) have been reported by Troll.[4] Compared to the reduction potential of parent Ph_2Tz, a lower value by 0.09 V is found for the difluoro derivative, $(FPh)_2Tz$, and 0.11 V for the dichloro derivative, $(ClPh)_2Tz$. Here, it is easier to reduce the tetrafluoro derivative by 0.18 V compared to the parent tetrazine Ph_2Tz.

Table 2. Redox potentials (*vs.* FcH^+/FcH) determined by cyclic voltammetry for diphenyl-*s*-tetrazine and halogenated analogues.

Compound	E_c^{red1} / V	E_a^{red1} / V	$E_{1/2}^{red1}$ / V	ΔE^{red1} / mV	I_c/I_a	Difference [a] $\Delta E_{1/2}^{red1}$	$E_{1/2}^{ox1}$ / V	E_c^{red2} / V
Ph_2Tz	−1.33	−1.23	−1.28	100	0.96		+1.59 [c]	–
$(FPh)_2Tz$ [b]			−1.19			+0.09		
$(F_2Ph)_2Tz$	−1.14	−1.05	−1.10	90	0.99	+0.18	–	−2.48 [d]
$(ClPh)_2Tz$ [b]			−1.13			+0.15		

[a] Difference in V between $E_{1/2}^{red1}$ for Ph_2Tz and $E_{1/2}^{red1}$ for the halogenated tetrazine.

[b] Troll, 1982 (ref. 4).

[c] Irreversible wave with $I_c/I_a = 0.86$.

[d] Irreversible wave with no anodic wave observed.

Surprisingly, a quasi-reversible oxidation wave was observed for the parent tetrazine here, Ph_2Tz, at $E_{1/2}$ 1.59 V versus the ferrocene/ferrocenium couple at 0.0 V as shown in Figure S5. Such an oxidation wave was not observed for $(FPh)_2Tz$ within the acetonitrile solvent window. By contrast, $(F_2Ph)_2Tz$ showed an irreversible second reduction peak with a cathodic wave at -2.48 V. A second reduction wave was not observed for Ph_2Tz which is presumably outside the solvent window. The irreversibility of the second reduction peak of some tetrazine derivatives has been associated to the fast protonation reaction of the strongly basic dianion by traces of residual water or even

by acetonitrile.[4] In CH_2Cl_2, which is more acidic than CH_3CN, even the first reduction peaks of Ph_2Tz and $(FPh)_2Tz$ are found to be irreversible.

UV-Vis absorption spectroscopy. UV-Vis spectra for Ph_2Tz and $(F_2Ph)_2Tz$ in *n*-hexane solution are displayed in Figure 3. The experimental energy value of the electronic transitions together with the molar absorption coefficients (ε) determined in different solvents (*n*-hexane, methanol, CCl_4, $CHCl_3$ and CH_2Cl_2) are shown in Table 3 for both molecules. The weak, visible band $n \rightarrow \pi^*$ for tetrazine derivatives does not show any significant shift upon fluorination of the phenyl rings. This is due to the fact that the transition mainly involves HOMO (b_{3g}) and LUMO (a_u), both fully localized on the tetrazine ring (see Figures S6 and S7) and, hence, the substituents have a reduced effect on its energy (Table S10). In contrast, the intense band $\pi \rightarrow \pi^*$, appeared at 4.3 eV for $(F_2Ph)_2Tz$, most involves HOMO-1 (b_{2g}) and LUMO+1 (b_{3u}), both delocalized throughout the molecule and thus the presence of fluorine atoms brings on a blue shift of 0.1 – 0.2 eV (Figure S7 and Table S11). The solvent effect was also analyzed within the PCM model and, as a result, calculated and experimental energies for $b_{3g} \rightarrow a_u$ (n, π^*) transition fit closely each other keeping differences not larger than 0.10 eV (see Table S12). MP2/6-31+G* geometry reduces those differences up to 0.03 eV or even less (see Table 3). For the $b_{2g} \rightarrow b_{3u}$ (π, π^*) transition, a worse fitting between experimental and theoretical values was observed, TD-PBE0/6-31+G*//MP2/6-31+G* being again the level which behaves best with differences of *ca.* 0.3 eV (see Tables 3 and S12). Those differences between experimental and calculated energies are within the expected accuracy for TD-PBE0. For instance, in the extensive TD-DFT benchmark reported by Jacquemin et al.[80] and a later review by Laurent and Jacquemin,[81] TD-PBE0 appears as one of the most accurate TD-DFT methods to calculate vertical electronic transitions with mean absolute deviations (MAD) of 0.22 eV[80] and 0.24 eV.[81]

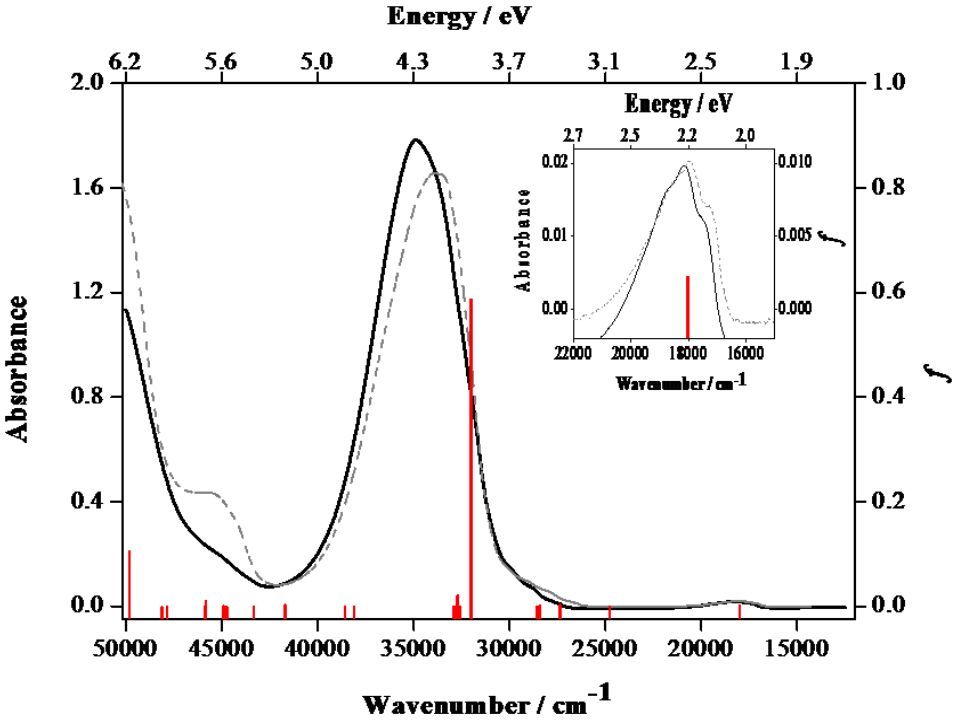

Figure 3. UV-Vis spectra recorded for $(F_2Ph)_2Tz$ (black line) and Ph_2Tz (gray and dotted line) in *n*-hexane solution. The concentrations of the solutions were 5.4×10^{-5} and 5.6×10^{-5} mol L^{-1}, respectively. The red bars correspond to the oscillator strengths (*f*) calculated for the electronic transitions of $(F_2Ph)_2Tz$ in *n*-hexane solution at the TD-PBE0/6-31+G*//MP2/6-31+G* level within the PCM methodology.

Table 3. Energy ($E_{exp.}$) and molar absorption coefficient (ε) of the different bands found in the UV−Vis spectra of Ph_2Tz and $(F_2Ph)_2Tz$ in various solvents along with the energy calculated ($E_{calc.}$) for the main electronic transitions of $(F_2Ph)_2Tz$ at the TD-PBE0/6-31+G*//MP2/6-31+G* level within the PCM methodology.

Intensity [a]	Solvent	$E_{exp.}$ / eV		ε / L mol^{-1} cm^{-1}		$E_{calc.}$ / eV	Assignment
		Ph_2Tz	$(F_2Ph)_2Tz$	Ph_2Tz	$(F_2Ph)_2Tz$	$(F_2Ph)_2Tz$	$(F_2Ph)_2Tz$
	CH_2Cl_2	2.27 [b]	2.29	–	498		
	$CHCl_3$	2.25 [c]	2.28	481 [c]	538		
w	CCl_4	2.23 [c]	2.26	565 [c]	506	2.24	$b_{3g} \rightarrow a_u$ (n,π^*)
	CH_3OH	2.28 [c]	2.32	376 [c]	401	2.29	$b_{3g} \rightarrow a_u$ (n,π^*)
	n-Hexane	2.23 [c]	2.25	392 [c]	533	2.23	$b_{3g} \rightarrow a_u$ (n,π^*)
	CH_2Cl_2	–	(3.2-3.7)	–	–		
	$CHCl_3$	(3.3-3.7) [c]	(3.2-3.7)	–	–		
sh	CCl_4	(3.2-3.7) [c]	(3.3-3.7)	–	–		
	CH_3OH	(3.2-3.7) [c]	(3.3-3.8)	–	–		
	n-Hexane	(3.3-3.7) [c]	(3.3-3.8)	–	–		

	CH_2Cl_2	4.16 [b]	4.28	–	33210		
	$CHCl_3$	4.13 [c]	4.26	33327 [c]	35170		
s	CCl_4	4.08 [c]	4.28	38513 [c]	30729	4.01	$b_{2g}\rightarrow b_{3u}(\pi,\pi^*)$
	CH_3OH	4.20 [c]	4.34	32043 [c]	33268	4.08	$b_{2g}\rightarrow b_{3u}(\pi,\pi^*)$
	n-Hexane	4.18 [c]	4.32	32937 [c]	32272	3.97	$b_{2g}\rightarrow b_{3u}(\pi,\pi^*)$
	CH_2Cl_2	–	–		–		
	$CHCl_3$	–	–	–	–		
sh	CCl_4	–	–	–	–		
	CH_3OH	5.65 [c]	5.62	–	–		
	n-Hexane	5.64 [c]	(5.2-5.8)	–	–		

[a] Intensity: (w) weak; (s) strong; (sh) shoulder

[b] Kurach et al., 2011. Reference 82.

[c] Moral et al., 2012. Reference 8.

Spectroelectrochemistry. Figure 4 shows the UV-Vis-NIR spectra for neutral and monoanion species of Ph_2Tz and $(F_2Ph)_2Tz$ in CH_3CN solutions. Table 4 lists the assignments and energies predicted at TD-PBE0/6-31+G*//PBE0/6-31+G* level within the PCM approximation for the single anions. A broad, very weak band for both anion species appears between 1.7 and 2.2 eV and it is assigned to a $\pi \rightarrow \pi^*$ transition involving SOMO α (a_u) at the tetrazine ring and LUMO α (b_{3u}) which is delocalized over all three rings (Figures 4, S6 and S7). The weak, visible band at *ca.* 2.3 eV for the monoanions is assigned to an $n \rightarrow \pi^*$ transition. This transition mainly involves HOMO-1 β (b_{3g}) and LUMO β (a_u) at the tetrazine ring and hence does not display any significant energy shift with the fluorine atoms.

A new band for $[(F_2Ph)_2Tz]^-$ (a shoulder for $[Ph_2Tz]^-$) can be seen at *ca.* 3.4 eV which has been assigned to a SOMO α (a_u) → LUMO+2 α (b_{1g}) transition. The LUMO+2 α is located at the terminal aryl groups and thus this transition is influenced by the fluorine atoms. This effect is shown by the significant shift of this band as compared to the corresponding one for the Ph_2Tz monoanion. The intense band π (b_{2g}) → π^*(b_{3u}) from neutral species corresponds to HOMO-2 α → LUMO α and HOMO-2 β → SOMO β transitions for the anionic ones.

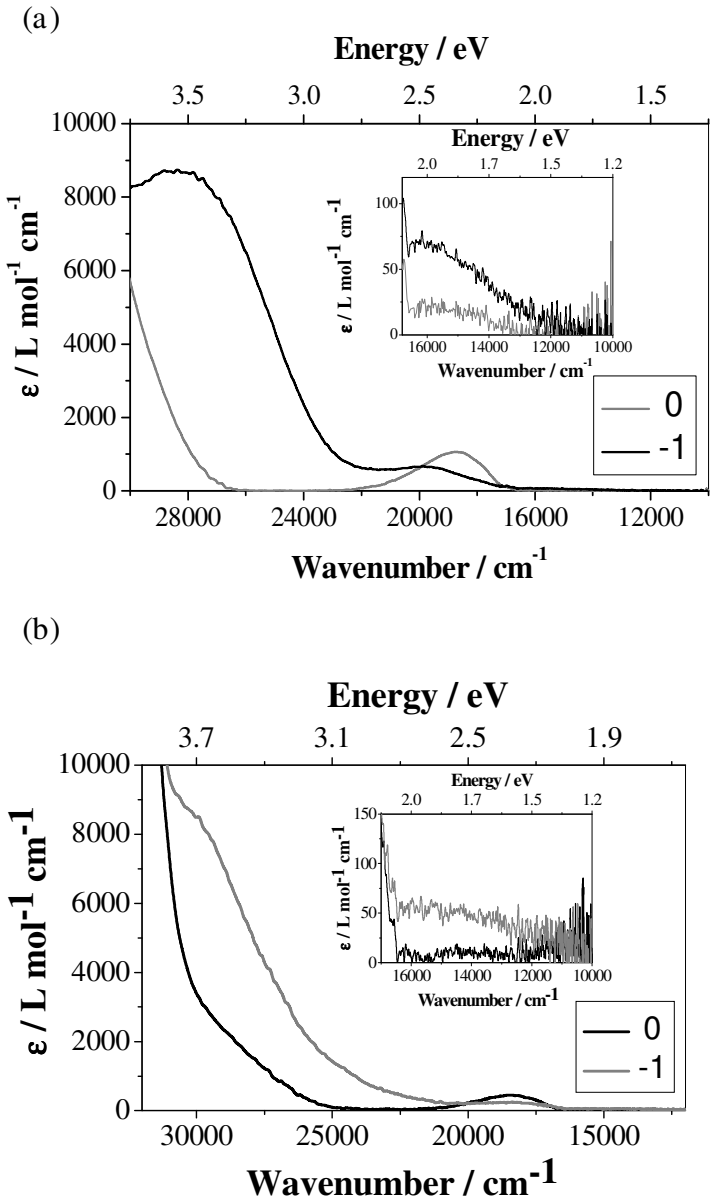

Figure 4. UV-Vis spectra recorded for the neutral and monoanionic species of Ph_2Tz (top) and $(F_2Ph)_2Tz$ (bottom) in acetonitrile using an OTTLE spectroelectrochemical cell.

Table 4. Energy and assignment of the main bands found in the UV−Vis spectra of the monoanionic species $[Ph_2Tz]^-$ and $[(F_2Ph)_2Tz\ ]^-$.

Compound	E / eV [a]	ε [c]	Transition	E / eV [d]	*f*	Main component of the transition (% contribution) [d]
$[Ph_2Tz]^-$	[2.0] [b]	70	$a_u \rightarrow b_{3u}$ (π,π^*)	1.26	0.0000	SOMO α → LUMO α (96%)
	2.25	230	$b_{3g} \rightarrow a_u$ (n,π^*)	2.53	0.0042	HOMO-1 β→LUMO β (92%)
			$a_u \rightarrow b_{2g}$ (π,π^*)	2.62	0.0039	SOMO α → LUMO+1 α (93%)
	[3.6] [b]	8500	$a_u \rightarrow b_{1g}$ (π,π^*)	3.02	0.0437	SOMO α → LUMO+2 α (94%)
	4.22	33900	$b_{2g} \rightarrow b_{3u}$ (π,π^*)	4.24	0.1214	HOMO-2 β → SOMO β (24%)
			$b_{2g} \rightarrow b_{3u}$ (π,π^*)	4.44	0.8841	HOMO-2 α → LUMO (61%)
						HOMO-2 β → SOMO β (25%)
$[(F_2Ph)_2Tz\ ]^-$	[2.0] [b]	70	$a_u \rightarrow b_{3u}$ (π,π^*)	1.10	0.0000	SOMO α → LUMO α (97%)
	2.42	650	$a_u \rightarrow b_{2g}$ (π,π^*)	2.45	0.0037	SOMO α → LUMO+1 α (95%)
			$b_{3g} \rightarrow a_u$ (n,π^*)	2.58	0.0043	HOMO-1 β→LUMO β (94%)
	3.50	8750	$a_u \rightarrow b_{1g}$ (π,π^*)	3.19	0.0348	SOMO α → LUMO+2 α (60%)
	4.40	36800	$b_{2g} \rightarrow b_{3u}$ (π,π^*)	4.27	0.1195	HOMO-2 β → SOMO β (23%)
			$b_{2g} \rightarrow b_{3u}$ (π,π^*)	4.47	0.8489	HOMO-2 α → LUMO α (60%)
						HOMO-2 β → SOMO β (26%)

[a] Experimental value in CH_3CN

[b] Broad band / shoulder

[c] Molar absorption coefficient (in units of L mol^{-1} cm^{-1})

[d] Calculated values at the TD-PBE0/6-31+G*//PBE0/6-31+G* level in CH_3CN

Electron transport related-properties. As stated before, the *n*-type semiconductor character of the series of studied molecular crystals was evaluated through their ease to electron injection and the efficiency of charge transport inside the material. Electron injection is mainly controlled by the energy difference between the work-function of the injecting metal and the (gas) ionization/affinity levels, HOMO/ LUMO, of the semiconductor for hole and electron injection, respectively, corrected for interface dipoles (see e.g. ref. 83,84). These dipoles come from either partial charge transfer metal-semiconductor, the reduction of the metal work function by the organic layer and the occupation of the metal-induced density of interface states in the gap of the organic material.[85,86] As a result, the gap between semiconductor affinity and ionization levels at the metal/organic interface narrows up to several eVs as compared to the gas-phase, frontier energy levels (see, e.g. ref. 84, 87 and 88). Any model aimed at a complete description of the metal/organic interface should account for those

specific interactions. Accordingly, the free, metal work function and the (gas) HOMO/LUMO levels do not give exact information but it is a guide about the alignment of levels at the interface and, therefore, for the electron/hole barrier injection and trends within a set of related compounds.[85] Thus, one can obtain qualitative information about charge injection efficiency through the Φ_m - $|E_{HOMO/LUMO}|$ difference.[85,89-91]

Calculated E_{LUMO}, EA and λ_i (inner reorganization energy) values for the series of tetrazine derivatives are shown in Figure 5 and Table 5. As stated before, the low LUMO energy facilitates a more efficient charge injection[19,20,26,31] and could also help the environmental stability of the material, although there is still no general guideline for predicting the air-stability of *n*-type organic semiconductors.[19,92] Within the studied series, the inclusion of halogen atoms lowers the E_{LUMO} up to *ca.* 0.6 eV with respect to Ph_2Tz and, hence, an easier electron injection can be expected. When the halogens are replaced with CN groups the E_{LUMO} is lowered further by 0.7 eV, reaching a value of −4.22 eV. For all studied compounds, injection barriers lower than 0.3 eV have been estimated with respect to some of the most commonly used electrodes, i.e. Na (= −2.6 eV), Ca (= −2.9 eV), Sm (= −2.7 eV) and Mg (= −3.7 eV).[93-96] Ohmic contact with the Al electrode (= −4.3 eV) is only expected for $((NC)_2Ph)_2Tz$.[97] Electron injection efficiency of an *n*-type organic semiconductor is also related to EA, which increases by ~0.7 eV (for adiabatic electron affinity, AEA) for haloderivatives with respect to Ph_2Tz (Table 5). The introduction of the CN group, a strong electron-withdrawing group, brings on the highest increase in EA (~1.4 eV for AEA). This fact has already been reported for pentacene, for which the introduction of a few CN groups raises the EA to values larger than those of perfluoropentacene, considered as a prototypical *n*-type OFET material.[26] The AEA value predicted for $((NC)_2Ph)_2Tz$ (2.86 eV) is near the

threshold value of 3.0 eV proposed for Newman et al.[31] to allow an efficient electron injection into the empty LUMO of a semiconductor molecule and the range of AEAs calculated at the same level of theory for pentacenes also including four CN groups (3.05 – 3.25 eV).[26] The high EA values calculated for the studied compounds gives an idea about the stability of the radical ion molecule toward quenching caused by molecular oxygen (the AEA calculated with B3LYP for O_2 is 0.59 eV while the experimental EA determined by photoelectron spectroscopy is 0.448 ± 0.006 eV).[63,98]

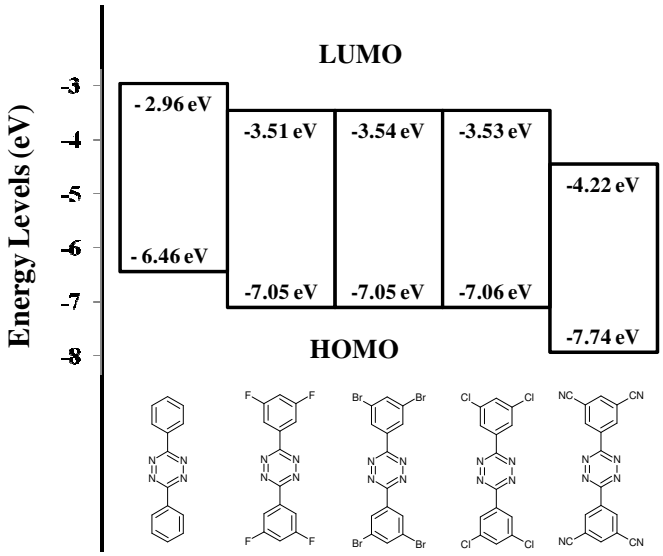

Figure 5. Calculated LUMO and HOMO energies at the B3LYP/6-31+G* level for the series of studied diphenyl-*s*-tetrazine derivatives.

Table 5. Adiabatic and vertical electron affinities (AEA, VEA) and λ_i calculated at the B3LYP/6-31+G* level for Ph_2Tz and $(X_2Ph)_2Tz$ (X = F, Cl, Br, CN) (units in eV).

Compound	AEA	VEA	λ_1	λ_2	λ_i
Ph_2Tz	1.51	1.22	0.30	0.29	0.60
$(F_2Ph)_2Tz$	2.16	1.84	0.22	0.31	0.53
$(Cl_2Ph)_2Tz$	2.15	1.85	0.31	0.30	0.61
$(Br_2Ph)_2Tz$	2.17	1.86	0.31	0.31	0.62
$((NC)_2Ph)_2Tz$	2.86	2.63	0.26	0.23	0.48

In general, the calculated λ_i values for the studied compounds (0.48 – 0.62 eV) look high compared to those published for typical *n*-type organic semiconductors, i.e. 0.24 eV for perfluoropentacene,[18] and 0.24 – 0.35 eV for a series of diimides studied by Chen et al. (calculated at the B3LYP/6-31++G** level).[44] $((NC)_2Ph)_2Tz$ and $(F_2Ph)_2Tz$ show the smallest λ_i values (0.53 and 0.48 eV, respectively) of the series (see Table 5), but in general the localized character of the LUMO orbital for all the selected diphenyl-*s*-tetrazine derivatives does not allow an easy charge excess accommodation. However, higher λ_i values are being reported for other small, π-conjugated molecules with halogen atoms such as fluoro and chloro tetrasubstituted oligothienoacenes.[99]

As concerns the electronic coupling parameter t_{12}, calculated values on the theoretically modeled Ph_2Tz and $(F_2Ph)_2Tz$ crystals are consistent with those calculated on the crystals from X-ray diffraction. Halogen substituents produce stronger overlapping between molecular orbitals of neighboring molecules, in such a way that t_{12} values for pathway 1 of $(F_2Ph)_2Tz$, $(Cl_2Ph)_2Tz$ and $(Br_2Ph)_2Tz$ become more than double those for Ph_2Tz and $((NC)_2Ph)_2Tz$ (see Figure 1 and Table 6). Ruiz Delgado et al.[14] also observed an increase in the electronic couplings for tetracene and pentacene crystals upon perfluorination, being the largest ones those for molecules stacked in a displaced cofacial configuration. In general, transfer integrals for the main pathway in each compound turn out to be higher than those calculated by Vaini et al.[100] at the B3LYP/TZP level for some oligoacenes including pentacene (5 – 15 meV). The transfer integrals calculated for pathway 1 in halogenated derivative crystals, *i.e.* 45 – 51 meV, are the same order of magnitude as the strongest couplings either calculated at the PW91PW91/6-31G* level for the diimides studied by Chen et al.[44] (21.6 – 87.5 meV) or for the perylene derivatives studied by Wang et al. (26 – 64 meV).[101] Di Donato et al.[102] have also reported t_{12} values for a series of diimides derivatives within the range 74 – 96

meV, calculated at the B3LYP/3-21G level. Both diimides and perylenes are two families of compounds which are currently being studied due to their potential *n*-type semiconductor character and successfully been incorporated in the fabrication of electronic devices.[103-106]

Table 6. Calculated t_{12} values for Ph_2Tz and $(X_2Ph)_2Tz$ (X = F, Cl, Br, CN) along with the estimated values for k_{ET}, D, μ and $\mu_{rel.}$ (see Figure 1 to visualize pathways). In parenthesis, t_{12} values calculated from X-Ray experimental structure.

Compound	Path	t_{12} / meV[a]	k_{ET} / s^{-1}	D / 10^{-4} cm^2 s^{-1}	μ / 10^{-3} cm^2 V^{-1} s^{-1}	$\mu_{rel.}$
Ph_2Tz	1	18 (21)	3.25×10^{11}			
	2	3 (4)	9.03×10^{9}			
	3	1 (1)	1.00×10^{9}			
	Global			1.42	5.53	1.0
$(F_2Ph)_2Tz$	1	45 (48)	2.88×10^{12}			
	2	3 (3)	1.28×10^{10}			
	3	0 (0)				
	Global			6.69	26.04	4.7
$(Cl_2Ph)_2Tz$	1	48	2.19×10^{12}			
	2	7	4.67×10^{10}			
	3	0				
	Global			5.88	22.87	4.1
$(Br_2Ph)_2Tz$	1	51	2.36×10^{12}			
	2	7	4.45×10^{10}			
	3	1	9.08×10^{8}			
	Global			6.75	26.25	4.7
$((NC)_2Ph)_2Tz$	1	22	8.84×10^{11}			
	2	12	2.63×10^{11}			
	3	0				
	Global			3.40	13.22	2.4

[a] Only the pathways with the highest calculated electron couplings are collected in the table.

Absolute values for the electron-transfer rate constant and charge mobility were calculated through eqns. (1) and (8) and are shown in Table 6. In general, the estimated drift mobilities (0.006 – 0.026 cm^2 V^{-1} s^{-1}) lie on the lower limit of the values experimentally determined for common *n*-type organic semiconductors. For instance, in an exhaustive review on *n*-type organic semiconductors reported by Usta et al.,[107] experimental μ values measured in vacuum for electron-deficient N,N´-substituted

arylenediimides and perfluoroalkyl oligothiophenes turn out to be in the range 0.02 – 0.35 $cm^2\ V^{-1}\ s^{-1}$ and 0.03 – 1.7 $cm^2\ V^{-1}\ s^{-1}$, respectively. Nevertheless, we must emphasize that the comparison between experimental and theoretical mobilites is far from trivial due to the approximations assumed in the theoretical model used. Comparison with other theoretical μ values is not an easy task either due to the large number of methodologies used in literature such as mobility estimations for dimers only through the stacking direction, resolution anisotropic mobility calculations and applying the eqn. (6) for which D is calculated considering all the relative arrangements of neighboring molecules in the crystal. Geng et al., employing the MLJ formulation, calculated drift mobilities within 0.007 – 1.45 $cm^2\ V^{-1}\ s^{-1}$ for a set of perylene bisimide derivatives.[108] μ values between 0.08 and 0.34 $cm^2\ V^{-1}\ s^{-1}$ have been also calculated using a similar methodology for a set of naphthalene tetracarboxylic diimide derivatives.[109] In addition, Duan et al. have reported μ values within 0.26 – 3.38 $cm^2\ V^{-1}\ s^{-1}$ for series of cyanovinyl-substituted oligothiophenes using the MLJ model.[110] Again, the μ values calculated for the diphenyl-s-tetrazine derivatives lie on the lower limit of the theoretical values reported for some common *n*-type organic semiconductors and therefore high electron transport efficiencies should not be expected for these compounds.

Finally, the analysis of the effect of the substituent on the electron mobility is interesting in order to discuss new guidelines for the design of new *n*-type organic semiconductors. For an easier comparison, the relative charge mobilities ($\mu_{rel.}$) with respect to the parent compound, Ph_2Tz, have been also collected in Table 6. For all studied diphenyl-*s*-tetrazine derivatives, estimated relative mobilities are larger than 1.0, with values between 2.4 for $(Cl_2Ph)_2Tz$ and 4.7 for $(F_2Ph)_2Tz$ and $(Br_2Ph)_2Tz$. This fact can be attributed to two main factors: (i) the generally expected increase in the λ_i value

as a result of the functionalization with halogen atoms[14,18,99] does not occur due to the strong, localized LUMO on the *s*-tetrazine ring, (ii) halogen and CN group functionalization leads to a crystal structure modification providing an improvement on charge transfer integrals.

CONCLUSIONS

In this study, the opto-electronic properties and *n*-type semiconductor character of a series of 3,5-diphenyl-*s*-tetrazine derivatives including F, Cl, Br and CN substituents, $(X_2Ph)_2Tz$, have been investigated. Also, structural, spectroscopic, electrochemical and theoretical studies were carried out on the new compound, bis(3,5-difluorophenyl)-*s*-tetrazine, $(F_2Ph)_2Tz$, and compared with data for the parent bis(phenyl)-*s*-tetrazine Ph_2Tz. In the crystal, the $(F_2Ph)_2Tz$ molecules are in a T-shaped π-stacking arrangement as opposite to the herringbone one observed for Ph_2Tz. The crystal structures of the rest of the tetrazines, *i.e.* $(Cl_2Ph)_2Tz$, $(Br_2Ph)_2Tz$ and $((NC)_2Ph)_2Tz$ were theoretically modeled. The π-stacking parameters increase as a function of the substituent size thus the π-π interactions become less pronounced in the crystals on going from F to CN. The higher depolarization ratios determined for $(F_2Ph)_2Tz$ in the Raman spectrum with respect to Ph_2Tz indicates a higher deviation from the D_{2h} symmetry for the substituted compound in liquid phase. Cyclic voltammetry studies showed that $(F_2Ph)_2Tz$ is more easily reduced than Ph_2Tz by 0.18 V due to the electron-withdrawing fluorine atoms. The characteristic weak $n \rightarrow \pi^*$ and strong $\pi \rightarrow \pi^*$ bands were assigned to HOMO (b_{3g}) → LUMO (a_u) and HOMO-1 (b_{2g}) → LUMO+1 (b_{3u}) transitions for both compounds. TD-PBE0/6-31+G* yields a suitable spectrum prediction for low energy bands, especially when the geometry is previously optimized at the MP2/6-31+G* level including solvent effects. For the corresponding

anionic species, very low energy bands (1.7 – 2.2 eV) appear, which are assigned to a π → π* transition involving SOMO α (a_u) and LUMO (b_{3u}). The characteristic bands described for the neutral species do not suffer a significant energy shift.

As concerns *n*-type semiconducting character, $((NC)_2Ph)_2Tz$ should exhibit the more suitable electron injection properties, followed by the halogenated derivatives. In general, an ohmic contact with some of the most common electrodes has been predicted for all $(X_2Ph)_2Tz$ compounds. On the other hand, the highest electron couplings between neighbor molecules in the crystal as well as the highest mobility value has been estimated for $(Br_2Ph)_2Tz$. A closed mobility value was also estimated for $(F_2Ph)_2Tz$. Hence, the most efficient electron transport could be expected for both the fluorinated and brominated derivatives. Anyhow, estimated drift mobilities are in the lower limit of the experimental and theoretical values reported for common *n*-type organic semiconductors and therefore high electron transport efficiencies should not ordinarily be expected for diphenyl-*s*-tetrazine derivatives.

ASSOCIATED CONTENT

Supporting Information

Complete Refs. (14), (19), (49), (89) and (105); synthesis of bis(3,5-difluorophenyl)-s-tetrazine, $(F_2Ph)_2Tz$ (Scheme S1); atom numbering for bis(3,5-difluorophenyl)-s-tetrazine, $(F_2Ph)_2Tz$, (Chart S1); most relevant geometrical parameters extracted from the X-ray diffraction structure and the theoretically modeled crystals (Figure S1); molecular structures of Ph_2Tz and $(F_2Ph)_2Tz$ (Figure S2); IR spectra recorded for $(F_2Ph)_2Tz$ in CCl_4 solution and in solid phase with ATR (Figure S3); Raman spectrum recorded for $(F_2Ph)_2Tz$ in solid phase (Figure S4); cyclic voltammograms for Ph_2Tz and

$(F_2Ph)_2Tz$ (Figure S5); shape of the frontier molecular orbitals calculated for Ph_2Tz and $[Ph_2Tz]^-$ at the PBE0/6-31+G* level and with CH_3CN as solvent (Figure S6); shape of the frontier molecular orbitals calculated for $(F_2Ph)_2Tz$ and $[(F_2Ph)_2Tz]^-$ at the PBE0/6-31+G* level and with CH_3CN as solvent (Figure S7); crystal data and refinement parameters for compounds Ph_2Tz and $(F_2Ph)_2Tz$ (Table S1); bond lengths for Ph_2Tz (Table S2) and $(F_2Ph)_2Tz$ (Table S3); bond angles for Ph_2Tz (Table S4) and $(F_2Ph)_2Tz$ (Table S5); selected torsion angles for Ph_2Tz (Table S6) and $(F_2Ph)_2Tz$ (Table S7); geometrical parameters extracted from the X-ray diffraction structures and the theoretically modelled crystals (Table S8); vibrational assignment of the most representative bands found in the IR and Raman spectra of $(F_2Ph)_2Tz$ (Table S9); PBE and PBE-D mean absolute deviations (MAD) and errors (MAE) of lattice parameters for Ph_2Tz and $(F_2Ph)_2Tz$ (Table S10); electronic transitions computed for $(F_2Ph)_2Tz$ at different levels of theory within the isolated molecule approximation and assignment (Table S11) and main electronic transitions computed for $(F_2Ph)_2Tz$ in different solvents at the TD-PBE0/6-31+G* level on different geometries within the PCM methodology (Table S12). This material is available free of charge via the Internet at http://pubs.acs.org.

AUTHOR INFORMATION

Corresponding Author

* E-mail: mfg@ujaen.es.

ACKNOWLEDGMENTS

We (M. Moral, G. García, A. Garzón, J. M. Granadino-Roldán, M. Fernández-Gómez) gratefully acknowledge financial support from Junta de Andalucía (PAI-FQM

337 2013 contract) and Prof. J. Kirkpatrick (Oxford University) for the use of the J-from-g03 code. We (M. Melguizo, A. Peñas) also thank the Spanish Ministry of Science & Innovation, and Junta de Andalucía for financial support (grants MAT2009-14185-C02-01, P09-FQM-4765) and a fellowship to A. Peñas.

REFERENCES

(1) Katritzky, A. *Handbook of heterocyclic chemistry*. Pergamon Press. New York. **1986**.

(2) Gong, Y.H.; Audebert, P; Tang, J; Miomandre, F; Clavier, G; Badré, S; Méallet-Renault, R; Marrot, J. New tetrazines substituted by heteroatomos incluiding the first tetrazine based cyclophane: Synthesis and electrochemical properties. *J. Electroanal. Chem*. **2006**, *592*, 147 – 152.

(3) Clavier, G; Audebert, P. s-Tetrazine as building blocks for new functional molecules and molecular materials. *Chem. Rev*. **2010**, *110*, 3299 – 3314.

(4) Troll, T. Reduction potentials of substituted as-triazines and s-tetrazines in acetonitrile. *Electrochim. Acta*. **1982**, *27*, 1311 – 1314.

(5) Audebert, P; Miomandre, F.; Clavier, G.; Vernières, M. C.; Badré, S.; Méallet-Renault, R. Synthesis and properties of new tetrazines substituted by heteroatmos: Towards the world's smallest organic fluorophores. *Chem. Eur. J*. **2005**, *11*, 5667 – 5673.

(6) Plugge, M.; Alain-Rizzo, V.; Audebert, P.; Brouwer, A.M. Excited state dynamics of 3,6-diaryl-1,2,5,6-tetrazines. Experimental and theoretical studies. *J. Photochem. Photobiol. A: Chem*. **2012**, *234*, 12 – 20.

(7) Kaim, W. The coordination chemistry of 1,2,5,6-tetrazines. *Coord. Chem. Rev.* **2002**, *230*, 127 – 139.

(8) Moral, M.; García, G.; Peñas, A.; Garzón, A.; Granadino-Roldán, J. M.; Melguizo, M.; Fernández-Gómez, M. Electronic properties of diphenyl-s-tetrazineadn some related oligomers. An spectroscopic and theoretical study. *Chem. Phys*. **2012**, *408*, 17 – 27.

(9) Waluk, J.; Spanget-Larsen, J.; Thulstrup, E. Electronic states of symmetrically disubstituted s-tetrazines. *Chem. Phys*. **1995**, *200,* 201 – 2013.

(10) Qing, Z.; Audebert, P.; Clavier, G.; Miomandre, F.; Tang, J.; Vu, T.T.; Méallet-Renault, R. Tetrazines with hindered or electron withdrawing substituents: Synthesis, electrochemical and fluorescence properties. *J. Electroanal. Chem*. **2009**, *632*, 39 – 44.

(11) Gong, Y.H.; Miomandre, F.; Méallet-Renault, R.; Badré, S.; Galmiche, L.; Tang, T.; Audebert, P.; Clavier, G. Synthesis and physical chemistry of s-tetrazines: Which ones are fluorescent and why?. *Eur. J. Org. Chem*. **2009**, *2009*, 6121 – 6128.

(12) Moral, M.; Granadino-Roldán, J.M.; Garzón, A.; García, G.; Fernández-Gómez, M. Does the number of nitrogen atoms have an influence on the conducting properties of diphenylazines? A DFT insight. *Chem. Phys*. **2011**, *379*, 51 – 56.

(13) Audebert, P.; Sadki, S.; Miomandre, F.; Clavier, G.; Vernières, M.C.; Saoud, M.; Hapiot, P. Synthesis of new substituted tetrazines: electrochemical and spectroscopic properties. *New. J. Chem*. **2004**, *28,* 387 – 392.

(14) Ruiz-Delgado, M. C.; Pigg, K. R.; da Silva Filho, D. A.; Gruhn, N.E.; Sakamoto, Y.; Suzuki, T.; Malavé Osuna, R.; Casado, J.; Hernández, V.; López Navarrete, J.T.; et al. Impact of perfluorination of the charge-transport parameters of oligoacene crystals. *J. Am. Chem. Soc*. **2009**, *131,* 1502 – 1512.

(15) Koh, S. E.; Risko, C.; da Silva Filho, D. A.; Kwon, O.; Fachetti, A.; Brédas, J. L.; Marks, T. J.; Ratner, M. A. Modelling electron and hole transport in fluoroarene-oligothiopene semiconductors: investigation of geometric and electronic structure properties. *Adv. Funct. Mater*. **2008**, *18*, 332 – 340.

(16) Sakamoto, Y.; Suzuki, T.; Miura, A.; Fujikawa, H.; Tokito, S.; Taga, Y. Synthsis, Characterization, and electron-transport properties of perfluorinated phenylene dendrimers. *J. Am. Chem. Soc.* **2000**, *122*, 1832 –1833.

(17) Yoon, M.H.; Facchetti, A.; Stern, C.E.; Marks, T.J. Fluorocarbon-modified organic semiconductors: Molecular architecture, electronic and crystal structure tuning of arene- versus fluoroarene-thiophene oligomer thin-film properties. *J. Am. Chem. Soc.* **2006**, *128*, 5792 – 5801.

(18) Chen, H. Y.; Chao, I. Effect of perfluorination on the charge-transport properties of semiconductors: density functional theory study of perfluorinated pentacene and sexithiophene. *Chem. Phys. Lett*. **2005,** *401*, 539 – 545.

(19) Schmidt, R.; Oh, J.H.; Sun, Y-S.; Deppisch, M.; Krause, A.M.; Radacki, K.; Braunscheweig, H.; Konemann, M.; Erk, P.; Bao, Z.; et al. High-performance air-

stable n-channel organic thin film transistor based on halogenated perylene bismide semiconductors. *J. Am. Chem. Soc.* **2009**, *131*, 6215 – 6228.

(20) Wang, Y.; Parkin, S.R.; Gierschner, J.; Watson, M.D. Highly fluorinated benzobisbenzothiophenes. *Org. Lett.* **2008**, *10*, 3307 – 3310.

(21) Chai, S.; Wen, S.H.; Huang, J.D.; Han, K.L. Density functional theory study on electron and hole transport properties of organic pentacene derivatives with electron-withdrawing substituent. *J. Comput. Chem*. **2011**, *32*, 3218 – 3225.

(22) Inoue, Y.; Sakamoto, Y.; Suzuki, T.; Kobayashi, M.; Gao, Y.; Tokito, S. Organic Thin-Film Transistor with high electron mobility based on perfluoropentacene. *Jpn. J. Appl. Phys. Part 1*. **2005**, *44*, 3663 – 3668.

(23) Sakamoto, Y.; Suzuki, T.; Kobayashi, M.; Gao, Y; Fukai; Inoue, Y.; Sato, F.; Tokito, S. Perfluoropentacene: High-performance p-n junctions and complementary circuits with pentacene. *J. Am. Chem. Soc.* **2004**, *126*, 8138 – 8140.

(24) Tang, M. L.; Oh, J. H.; Reichardt, A. D.; Bao, Z. Chlorination: A general route toward electron transport in organic semiconductors. *J. Am. Chem. Soc*. **2009**, *131*, 3733 – 3740.

(25) Ming, L.; Tang, S.; Bao, Z. Halogenated materials as organic semiconductors. *Chem. Mater*. **2011**, *23*, 446 – 455.

(26) Kuo, M. Y.; Chen, H-Y.; Chao, I. Cyanation: Providing a three-in-one advantage for the design of n-type organic field-effect transistors. *Chem. Eur. J.* **2007**, *13*, 4750 – 4758.

(27) Pinner, A. Ueber die einwirkung von hydrazin auf imidoäther. *Justus Liebigs Ann. Chem.* **1897**, *297*, 221 – 271.

(28) Dolomanov, O.V.; Bourhis, L.J.; Gildea, R.J.; Howard, J.A.K.; Puschmann, H. OLEX2: A complete structure solution, refinement and analysis program. *J. Appl. Cryst.* **2009**, *42*, 339 – 341.

(29) Sheldrick, G.M. A short history of SHELX. *Acta Cryst*. **2008**, *A64*, 112 – 122.

(30) Krejčík, M.; Daněk, M.; Hartl, F. Simple construction of an infrared optically transparent thin-layer electrochemical cell: applications to the redox reactions of ferrocene, $Mn_2(CO)_{10}$ and $Mn(CO)_3$(3,5-di-t-butyl-catecholate)$^-$. *J. Electroanal. Chem.* **1991**, *317*, 179 – 186.

(31) Newman, C. R.; Frisbie, C. D.; da Silva Filho, D. A.; Brédas, J. L.; Ewbank, P. C.; Mann, K. R. Introduction of organic thin film transistors and design of n-channel organic semiconductors. *Chem. Mater*. **2004**, *16*, 4436 – 4451.

(32) Wang, L.; Nan, G.; Yang, X.; Peng, Q.; Li, Q.; Shuai, Z. Computational methods for design of organic materials with high charge mobility. *Chem. Soc. Rev*. **2010**, *39*, 423 – 434.

(33) Chen, X-K.; Zou, L-Y.; Huang, S.; Min, C-G.; Ren, A-M. ; Feng, J-K. Theoretical investigation of charge injection and transport properties of novel organic semiconductor materials-cyclic oligothiophenes. *Org. Electron*. **2011**, *12*, 1198 – 1210.

(34) Koch, N. Organic electronic devices and thier functional interfaces. *Chem. Phys. Chem*. **2007**, *8*, 1438 – 1455.

(35) Lindell, L.; Burquel, A.; Jakobsson, F.L.E.; Lemaur, V.; Berggren, M.; Lazzaroni, R.; Cornil, J.; Salaneck, W.R.; Crispin, X. P. Transparent, plastic, low-work-funtion poly(3,4-ethilendioxythiophene) electrodes. *Chem. Mater*. **2006**, *18*, 4246 – 4252.

(36) Davids, P.S.; Campbell, I.H.; Smith, D. L. Device model for single carrier organic diodes. *J. Appl. Phys.* **1997**, *82*, 6319 – 6325.

(37) Al Attar, H.A.; Monkman, A.P. Dopant effect on the charge injection, transport and devices efficiency of an electrophosphorescent polymeric light-emitting device. *Adv. Funct. Mater.* **2006**, *16*, 2231 – 2242.

(38) Marcus, R.A. Electron transfer reaction in chemistry. Theory and experiment. *Rev. Mod. Phys.* **1993**, *65*, 599 – 610.

(39) Barbara, P.F.; Meyer, T.J.; Ratner, M.A. Contemporary issues in electron transfer research. *J. Phys. Chem.* **1996**, *100*, 13148 – 13168.

(40) Troisi, A. Charge transport in high mobility molecular semiconductors: classical model and new theories. *Chem. Soc. Rev*. **2011**, *40*, 2347 – 2358.

(41) Brédas, J.L.; Beljonne, D.; Coropceanu, V.; Cornil, J. Charge-transfer and energy-transfer process in π-conjugated oligomers and polymers: a molcular picture. *Chem. Rev*. **2004**, *104*, 4971 – 5004.

(42) Coropceanu, V.; André, J.M.; Malagoli, M.; Brédas, J.L. The role of vibronic interactions on intramolecular and intermolecular electron transfer in π-conjugated oligomers. *Theor. Chem. Acc*. **2003**, *110*, 59 – 69.

(43) Coropceanu, V.; Cornil, J.; da Silva Filho, D.A.; Olivier, Y.; Silvey, R.; Brédas. J.L. Charge transport in organic semiconductors. *Chem. Rev*. **2007**, *107*, 926 – 952.

(44) Chen, X.K.; Zou, L.Y.; Guo, J.F.; Ren, A.M. An efficient strategy for designing n-type organic semiconductor materials-introducing a six-membered imide ring into aromatic diimides. *J. Mater. Chem*. **2012**, *22*, 6471 – 6484.

(45) Becke, A.D. Density-functional thermochemistry III. The role of exact exchange. *J. Chem. Phys*. **1993**, *98*, 5648 – 5652.

(46) Lee, C.; Yang, W.; Parr, R.G. Development of the Colle-Salvetti correlation-energy formula into a functional of the electron density. *Phys. Rev. B*. **1988**, *37*, 785 – 789.

(47) Perdew, J.P.; Burke, K.; Ernzerhof, M. Generalized gradient approximation made simple. *Phys. Rev. Lett*. **1996**, *77*, 3865 – 3868.

(48) Adamo, C.; Barone, V. A TDDFT study of the electronic spectrum of s-tetrazine in the gas-phase and in aqueous solution. *Chem. Phys. Lett*. **2000**, *330*, 152 – 160.

(49) Frisch, M. J.; Trucks, G. W.; Schlegel, H. B.; Scuseria, G. E.; Robb, M. A.; Cheeseman, J. R.; Scalmani, G.; Barone, V.; Mennucci, B.; Petersson, G. A.; et al. GAUSSIAN 09. Revision B.01. Gaussian Inc. Wallingford CT. **2009.**

(50) Merrick, J.P.; Moran, D.; Radom, L. An evolution of harmonic vibrational frequency scale factors. *J. Phys. Chem. A*. **2007**, *111*, 11683 – 11700.

(51) Cossi, M.; Rega, N.; Scalmani, G.; Barone, V. Energies, structures, and electronic properties of molecules in solution with the C-PCM salvation model. *J. Comput. Chem*. **2003**, *24*, 669 – 681.

(52) Tomasi, J.; Mennucci, B.; Cammi, R. Quantum mechanical continuum solvation models. *Chem. Rev*. **2005**, *105*, 2999 – 3094.

(53) Garzón, A.; Granadino-Roldán, J.M.; Moral, M.; García, G.; Fernández-Liencres, M.P.; Navarro, A.; Peña-Ruiz, T.; Fernández-Gómez, M. Density functional theory study of the optical and electronic properties of oligomers based on phenyl-ethynyl-units linked to triazole, thiadiazole, and oxadiazole rings to be used in molecular electronics. *J. Chem. Phys*. **2010**, *132*, 064901 – 064912.

(54) García, G.; Granadino-Roldán, J.M.; Garzón, A.; Moral, M.; Peña-Ruiz, T.; Navarro, A.; Fernández-Liencres, M.P.; Fernández-Gómez, M. Theoretical study of bis(phenylethynyl)thienoacenes as precursors of molecular wires for molecular electronics. *J. Phys. Chem. C*. **2010**, *114*, 12325 – 12334.

(55) Jacquemin, D.; Perpète, E.A.; Scuseria, G.E.; Ciofini, I.; Adamo, C. TD-DFT performance for the visible absorption spectra of organic dyes: conventional versus long-range hybrids. *J. Chem. Theory Comput.* **2008**, *4*, 123 – 135.

(56) Head-Gordon, M.; Pople, J.A.; Frisch, M.J. MP2 energy evaluation by direct methods. *Chem. Phys. Lett*. **1988**, *153*, 503 – 506.

(57) Frisch, M.J.; Head-Gordon, M.; Pople, J.A. A direct MP2 gradient method. *Chem. Phys. Lett*. **1990**, *166*, 275 – 280.

(58) Frisch, M.J.; Head-Gordon, M.; Pople, J.A. Semi-direct algorithms for the MP2 energy and gradient. *Chem. Phys. Lett*. **1990**, *166*, 281 – 289.

(59) Head-Gordon, M.; Head-Gordon, T. Analytic MP2 frequencies without fifth-order storage. Theory and application to bifurcated hydrogen bonds in the water hesamer. *Chem. Phys. Lett.* **1994**, *220*, 122 – 128.

(60) Meier, R.J., Koglin, E. On the problem of theoretical evaluation of the rotational barrier in aromatics with adjacent conjugated group: benzaldehyde and N-methylbenzamide. *Chem. Phys. Lett*. **2002**, *353*, 239 – 243.

(61) Viruela, P.M.; Viruela, R.; Ortí, E. Difficulties of density functional theory in predicting the torsinal potential of 2,2'-bithiophene. *Int. J. Quant. Chem*. **1998**, *70*, 303 – 312.

(62) Jansson, E.; Jha, P.C.; Ågren, H. Density functional study of triazole and thiadiazole systems as electron transporting materials. *Chem. Phys*. **2006**, *330*, 166 – 177.

(63) Dreizler, R.M.; Providênca, J. *Density functional methods in physics*, Plenum Press, New York and London, **1985**.

(64) Foresman, J.B.; Frisch, A.E. *Exploring chemistry with electronic structure methods*, 2nd ed. Pittsburg: Gausssian. Inc. Pittsburgh. **1996**.

(65) Rienstra-Kiracofe, J.C.; Barden, C.J.; Brown, S.T.; Schaefer, H.F. Electron affinities of polycyclic aromatic hydrocarbons. *J. Phys. Chem. A*. **2001**, *105*, 524 – 528.

(66) Zhan, C.G.; Nichols, J.A.; Dixon, D.A. Ionization potential, electron affinity, electronegativity, hardness and electron excitation energy: molecular properties from density functional theory orbital energies. *J. Phys. Chem. A*. **2003**, *107*, 4184 – 4195.

(67) Coropceanu, V.; Malagoli, M.; da Silva Filho, D.A.; Gruhn, N.E.; Bill, T.G.; Brédas, J.L. Hole- and electron-vibrational couplings in oligoacene crystals: intramolecular contributions. *Phys. Rev. Lett*. **2002**, *89*, 275503 – 275507.

(68) Zhang, G.; Musgrave, C.B. Comparison of DFT methods for molecular orbital eigenvalue calculations. *J. Phys. Chem. A*. **2007**, *111*, 1554 – 1561.

(69) Grimme, S. Semiempirical GGA-type density functional constructed with a long-range dispersion correction**,** *J. Comput. Chem*. **2006,** *27*, 1787 –1799

(70) Soler, J.M.; Artacho, E.; Gale, J.D.; García, A.; Junquera, J.; Ordejón, P.; Sánchez-Portal D. The SIESTA method for ab initio order-N materials simulation. *J. Phys.: Condens. Matter*. **2002**, *14*, 2745 – 2779.

(71) Baumeier, B.; Kirkpatrick, J.; Andrienko, D. Density-functional based determination on intermolecular charge transfer properties for large-scale morphologies. *Phys. Chem. Chem. Phys*. **2010**, *12,* 11103 – 11113.

(72) Kirkpatrick, J. An approximate method for calculating transfer integrals based on the ZINDO Hamiltonian. *Int. J. Quantum Chem*. **2008**, *108*, 51 – 56.

(73) Ahmed, N.A.; Kitaigorodsky, A.I. Experimental and theoretical determination of the crystal structure of 3,6-diphenyl-s-tetrazine. *Acta Cryst*. **1972**, *B28*, 739 – 742.

(74) Holmes, D.; Kumaraswamy, S.; Matzger, A.J.; Vollhardt, K.P.C. On the nature of nonplanarity in the[N]Phenylenes. *Chem. Eur. J.* **1999**, *5*, 3399 – 3412.

(75) Infantes, L.; Mahon, M.F.; Male, L.; Raithby, P.R.; Teat, S.J.; Sauer, J.; Jagerovic, N.; Elguero, J.; Motherwell, S. 1,2,4,5-Tretrazines vs. carboxylic acid dimmers: molecular chemistry vs. supramolecular chemistry. *Helvetica Chim. Acta.* **2003**, *86,* 1205 – 1221.

(76) Oxtoby, N.S.; Blake, A.J.; Champness, N.R.; Wilson, C. The role of 1,2,4,5-tetrazine rings in π-π stacking interactions. *Cryst. Eng. Comm.* **2003**, *5*, 82 – 86.

(77) Hummer, K.; Pusching, P.; Ambrosch-Draxl, C. Ab initio study of anthracene under high pressure. *Phys. Rev. B*. **2003**, *67*, 184105 – 184112.

(78) Provencer, F.; Bérubé, N.; Lapdrade, J.F.; Simard, G.; Tant, J.; de Halleux, V.; Geerts, Y.; Silva, C.; Côté, M. Large electronic bandwidth in solution-processable pyrene crystals: the role of close-packed crystal structure. *J. Chem. Phys.* **2012**, *137*, 034706 – 034715.

(79) Hollas, J.M. *Modern Spectroscopy*, John Willey & Sons, **1987**.

(80) Jacquemin, D.; Wathelet, V; Perpète, E.A.; Adamo, C. Extensive TD-DFT benchmark: Singlet-excited states of organic molecules. *J. Chem. Theory Comput*. **2009**, *5*, 2420 – 2435.

(81) Laurent, A.D.; Jacquemin, D. TD-DFT benchmarks: A review. *Int. J. Quantum. Chem*. **2013**, *113*, 2019 – 2039.

(82) Kurach, E.; Djurado, D.; Rimarčik, J.; Kornet, A.; Wlostowski, M.; Lukeš, V.; Pécaut, J.; Zagorska, M.; Pron, A. Effect of substituents on redox, spectroscopic and structural properties of conjugated diaryltetrazines – a combined experimental and theoretical study. *Phys. Chem. Chem. Phys.,* **2011**, *13*, 2690 – 2700.

(83) McMahon, P.; Troisi, A. Evaluation of the external reorganization energy of polyacenes. *J. Phys. Chem. Lett.* **2010**, *1*, 941 – 946.

(84) Körzdörfer, T.; Parrish, R.M.; Sears, J.S.; Sherrill, C.D.; Brédas, J.L. On the relationship between bond-length alternation and many-electron self-interaction error. *J. Chem. Phys.* **2012**, *137*, 124305 – 124313.

(85) Cheng, X.; Noh, Y.Y.; Wang, J.; Tello, M.; Frisch, J.; Blum, R.P.; Vollmer, A.; Rabe, J.P.; Koch, N.T.; Sirringhaus, H. Controlling electron and hole charge injection in ambipolar organic field-effect transistors by self-assembled monolayers. *Adv. Funct. Mater*. **2009**, *19*, 2407 –2415.

(86) Amy, F.; Chan, C.; Kahn, A. Polarization at the gold/pentacene interface. *Org. Electron.* **2005**, *6*, 85 – 91.

(87) Natali, D.; Caironi, M. Charge injection in solution-processed organic field-effect transistors: physics, models and characterization methods. *Adv. Mater*. **2012**, *24*, 1357 – 1387.

(88) Crispin, X.; Geskin, V.; Crispin, A.; Cornil, J.; Lazzaroni, R.; Salaneck, W.R.; Brédas. J.L. Characterization of the interface dipole at organic/metal interfaces. *J. Am. Chem. Soc*. **2002**, *124*, 8131 – 8141.

(89) Wen, Y.; Liu, Y. Recent progress in n-channel organic thin-film transistors. *Adv. Mater*. **2010**, *22*, 1331 – 1345.

(90) Yan, L.; Zhao, Y.; Wang, X.; Wang, X.Z.; Wong, W.Y.; Liu, Y.; Wu, W.; Xiao, Q.; Wang, G.; Zhou, X.; et al. Platinum-based poly(aryleneethynylene) polymers containing thiazolothiazole group with high hole mobilities for field-effect transistors applications. *Macromol. Rapid Commun*. **2012**, *33*, 603 – 609.

(91) Ishii, H.; Sugiyama, K.; Ito, E.; Seki, K. Energy level alignment and interfacial electronic structures at organic/metal and organic/organic interfaces. *Adv. Mater.* **1999**, *11*, 605 – 625.

(92) Meng, Q.; Hu, W. Recent progress of n-type organic semiconducting small molecules for organic field-effect transistors. *Phys. Chem. Chem. Phys.* **2012**, *14*, 14152 – 14164.

(93) CRC, *Handbook of Chemistry and Physics*, CRS Press, Boca Raton, FL, **1995**.

(94) Yasuda, T.; Goto, T.; Fujita, K.; Tsutsui, T. Ambipolar pentacene field-effect transistors with calcium source-drain electrode. *Appl. Phys. Lett.* **2004**, *11*, 2098 – 2100.

(95) Koch, N.; Zojer, E.; Rajagopal, A.; Ghjsen, J.; Johnson, R.L.; Leising, G.; Pireaux, J-J. Electronic properties of the interface between the wide bandgap organic semiconductors *para*-sexiphenyl and samarium. Adv. *Funct. Mater.* **2001**, *11*, 51 – 58.

(96) Stössel, M.; Staudigle, J.; Steuber, F.; Simmerer, J.; Winnacker, A. Impact of the cathode metal work function on the performance of vacuum-deposited organic light emitting-devices. *Appl. Phys. A.* **1999**, *68*, 387 – 390.

(97) Khan, M.A.; Xu, W.; ul-Haq, K.; Zhang, X.W.; Bai, Y.; Jiang, X.Y.; Zhang, Z.L. Zhu, W.Q. Electron injection and transport mechanism in organic devices based on electron transport materials. *J. Phys. D: Appl. Phys*. **2008**, *41*, 225105 – 225110.

(98) Ervin, K.M.; Anusiewicz, I.; Skurski, P.; Simons, J.; Lineberger, W.C. The only stable state of O_2^- is the $X^2\Pi_g$ ground state and it (still!) has an adiabatic electron detachment energy of 0.45 eV. *J. Phys. Chem. A*. **2003**, *107*, 8521 – 8529.

(99) Zhang, Y.; Cai, X.; Bian, Y.; Li, X.; Jiang, J. Heteroatom substitution of oligothienoacenes: from good p-type semiconductors to good ambipolar semiconductors for organic field-effect transistors. *J. Phys. Chem. C.* **2008**, *112*, 5148 – 5159.

(100) Viani, L.; Olivier, Y.; Athanasopoulos, S.; da Silva Filho, D.A.; Hulliger, J.; Brédas, J.L.; Gierschner, J.; Cornil, J. Theoretical characterization of charge transport in one-dimensional collinear arrays of organic conjugated molecules. *Chem. Phys. Chem.* **2010**, *11*, 1062 – 1068.

(101) Wang, C.; Wang, F.; Yang, X.; Li, Q.; Shuai, Z. Theoretical comparative studies of charge mobilities for molecular materials: PET vs bnpery. *Org. Electron.,* **2008**, *9*, 635 – 640.

(102) Di Donato, E.; Fornari, R.P.; Di Motta, S.; Li, Y.; Wang, Z.; Negri, F. n-type charge transport and mobility of fluorinated perylene bisimide semiconductors. *J. Phys. Chem. B*. **2010**, *114*, 5327 – 5334.

(103) Tatemichi, S.; Ichikawa, M.; Koyama, T.; Taniguchi, Y. High mobility n-type thin-film transistors based on N,N'-ditridecyl perylene diimide with thermal treatments. *Appl. Phys. Lett*. **2006**, *89*, 112108 – 112110.

(104) Chesterfield, R.J.; McKeen, J.C.; Newman, C.R.; Ewbank, P.C.; da Silva Filho, D.A.; Brédas, J. L.; Miller, L.L.; Mann, K.R.; Frisbie, C.D. Organic thin film transistors based on N-Alkyl perylene diimides: charge transport kinetics as a function of gate voltage and temperature. *J. Phys. Chem. B.* **2004**, *108*, 19281 – 19292.

(105) Briseno, A.L.; Mannsfeld, S.C.B.; Reese, C.; Hancock, J.M.; Xiong, Y.; Jenekhe, S.; Bao, Z.; Xia, Y. Perylenediimide nanowires and their use in fabricating field-effect transistors and complementary inverters. *Nano Lett.* **2007**, *7*, 2847 – 2853.

(106) Sun, Y.; Tan, L.; Jiang, S.; Qian, H.; Wang, Z.; Yan, D.; Di, C.; Wang, Y.; Wu, W.; Yu, G. et al. D. High-performance transistor based on individual single-crystalline micrometer wire of perylo[1,12-b,c,d]thiophene. *J. Am. Chem. Soc.* **2007**, *129*, 1882 – 1883.

(107) Usta, H.; Facchetti, A.; Marks, T.J. n-Channel semiconductor materials design for organic complementary circuits. Acc. Chem. Res. **2011**, *44*, 501 – 510.

(108) Geng, Y.; Wang, J.; Wu, S.; Li, H.; Yu, F.; Yang, G.; Gao, H.; Su Z. Theoretical discussions on electron transport properties of perylene bisimide derivatives with different molecular packings and intermolecular interactions. *J. Mater. Chem.* **2011**, *21*, 134 – 143.

(109) Geng, Y.; Wu, S.X.; Li, H.B.; Tang, X.D.; Wu, Y.; Su Z.M.; Liao, Y. A theoretical discussion on the relationships among molecular packings, intermolecular interactions and electron transport properties for naphthalene tetracarboxylic diimide derivatives. *J. Mater. Chem*. **2011**, *21*, 15558 – 15566.

(110) Duan, Y.A.; Geng, Y.; Li, H.B.; Tang, X.D.; Jin, J.L.; Su, Z.M. Theoretical study on charge transport properties of cyanovinyl-substituted oligothiophenes. *Org. Electron.* **2012**, *13*, 1213 – 1222.